Please cite this article in press as: Blum et al., Stem Cell Factor-Based Identification and Functional Properties of In Vitro-Selected Subpopulations of Malignant Mesothelioma Cells, Stem Cell Reports (2017), http://dx.doi.org/10.1016/j.stemcr.2017.02.005

Stem Cell Reports
Article

ISSCR

OPEN ACCESS

Stem Cell Factor-Based Identification and Functional Properties of In Vitro-Selected Subpopulations of Malignant Mesothelioma Cells

Walter Blum,[1,*] László Pecze,[1] Emanuela Felley-Bosco,[2] Licun Wu,[3] Marc de Perrot,[3] and Beat Schwaller[1]
[1]Unit of Anatomy, Department of Medicine, University of Fribourg, Route Albert-Gockel 1, 1700 Fribourg, Switzerland
[2]Laboratory of Molecular Oncology, Lungen- und Thoraxonkologie Zentrum, University Hospital Zürich, Sternwartstrasse 14, 8091 Zürich, Switzerland
[3]Latner Thoracic Surgery Research Laboratories, Division of Thoracic Surgery, Toronto General Hospital, University Health Network, University of Toronto, Toronto, ON M5G 2C4, Canada
*Correspondence: walter-vincent.blum@unifr.ch
http://dx.doi.org/10.1016/j.stemcr.2017.02.005

SUMMARY

Malignant mesothelioma (MM) is an aggressive neoplasm characterized by a poor patient survival rate, because of rapid tumor recurrence following first-line therapy. Cancer stem cells (CSCs) are assumed to be responsible for initiating tumorigenesis and driving relapse after therapeutic interventions. CSC-enriched MM cell subpopulations were identified by an OCT4/SOX2 reporter approach and were characterized by (1) increased resistance to cisplatin, (2) increased sensitivity toward the FAK inhibitor VS-6063 in vitro, and (3) a higher tumor-initiating capacity in vivo in orthotopic xenograft and allograft mouse models. Overexpression of NF2 (neurofibromatosis 2, merlin), a tumor suppressor often mutated or lost in MM, did not affect proliferation and viability of CSC-enriched MM populations but robustly decreased the viability of reporter-negative cells. In contrast, downregulation of calretinin strongly decreased proliferation and viability of both populations. In summary, we have enriched and characterized a small MM cell subpopulation that bears the expected CSC characteristics.

INTRODUCTION

Malignant mesothelioma (MM) is a highly aggressive neoplasm most often linked to exposure to asbestos fibers, which induce chronic inflammation and perpetual tissue repair by the surrounding mesothelial cells. Chronic hyper-proliferation leads to a series of genetic and epigenetic modifications of these cells gradually developing into malignant cancer cells and tumor formation (Stahel et al., 2009). Therapy generally comprises a combination chemotherapy consisting of cisplatin (cis-Pt) and pemetrexed, at times accompanied by radiotherapy and/or tumor removal by surgery (Cho et al., 2014). The low success rate of treatments is likely caused by a subpopulation of tumor cells characterized by high resistance to chemotherapy and a high tumor-forming potential leading to rapid recurrence, the so-called cancer stem cells (CSCs). Currently no universal markers exist for unambiguously identifying CSCs in MM or other cancer types, possibly linked to the dynamic and heterogeneous properties of CSCs (Akrap et al., 2016). Various assays have been described to enrich CSC-containing tumor cell subpopulations: fluorescence-activated cell sorting (FACS) of putative CSCs, sometimes also called tumor-initiating cells (TICs), relies mostly on expression of cell surface markers (CD133, CD44, CD24; Klonisch et al., 2008; or EpCAM; Visvader and Lindeman, 2008) or on dye-exclusion assays based on the elevated expression of ABC transporter family members, e.g., ABCG2 (Hirschmann-Jax et al., 2004). Alternatively, increased aldehyde dehydrogenase (*ALDH1*) activity characterizes a subpopulation of cancer cells with CSC properties (D'Angelo and Wicha, 2010), also in human MM cell lines (Shapiro et al., 2014). The currently most comprehensive characterization of CSC subpopulations has allowed the identification of a hierarchical organization, where CSC subpopulations dynamically change between various differentiation states (clusters) (Akrap et al., 2016). Each cluster is characterized by a series of genes; CSCs expressing typical (normal) pluripotency stem cell marker genes such as *SOX2*, *NANOG*, and *OCT4* (also named *POU5F1*) were found at the apex of the hierarchy, followed by populations of one to several types of progenitor cell populations expressing genes such as *ALDH1* and *ABCG2*. Thus, CSC-enrichment methods based on stem cell marker expression including SOX2 and OCT4 have been particularly successful in selecting tumor cells with (1) the high tumor-forming potential in vivo, (2) the particular growth properties including self-renewal and asymmetric cell division, (3) the increased chemoresistance, and (4) the aggressiveness shown in other cancer types (Gangemi et al., 2009; Tang et al., 2015). The concept that CSCs within a tumor mass might represent important targets for therapy is now accepted for nearly all cancer types (Valent et al., 2012).

Here, we identified and characterized MM cell subpopulations in vitro based on their increased endogenous expression of SOX2 and OCT4 driving a reporter (EGFP) (Hotta et al., 2009; Tang et al., 2015). We demonstrate these cells to have different properties with respect to chemoresistance, and that the proportion of these cells appears to be determined intrinsically, also involving asymmetric cell division. Moreover, overexpression of the tumor suppressor NF2 caused an almost complete block of cell

Please cite this article in press as: Blum et al., Stem Cell Factor-Based Identification and Functional Properties of In Vitro-Selected Subpopulations of Malignant Mesothelioma Cells, Stem Cell Reports (2017), http://dx.doi.org/10.1016/j.stemcr.2017.02.005

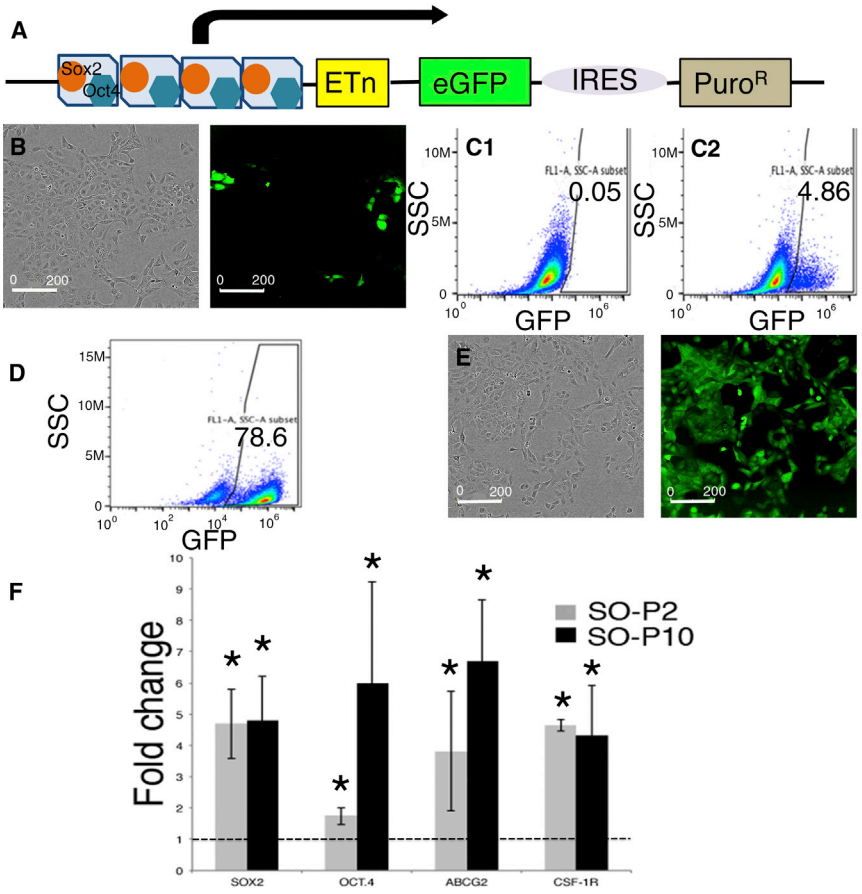

Figure 1. An EGFP Reporter-Based and Puromycin-Selected Subpopulation of ZL55 Cells Shows Higher Transcript Levels of CSC-Associated Genes

(A) Schematic representation of the pL-SIN-EOS-S(4+)-EiP lentiviral (LV) construct with OCT4 (blue) and SOX2 (orange) binding sites. Binding of OCT4 and SOX2 initiates expression of EGFP and Puro^R.

(B) A small percentage of EGFP(+) cells is present in LV-transduced ZL55 cells (left panel, bright field image; right panel, fluorescence image).

(C) FACS analysis reveals an EGFP(+) subpopulation of around 5% (C2); with the same gating only 0.05% of non-infected ZL55 cells are counted (C1).

(D) Directly after puromycin selection stringent FACS analysis of ZL55-SO-P2 cells identifies 78.6% of cells as EGFP(+).

(E) Puro^R selection results in a visibly 100% positive EGFP(+) ZL55-SO-P2 subpopulation (right); left image: bright field image of the same cells.

(F) qRT-PCR reveals a 4.5-fold increase for *SOX2* expression in ZL55-SO-P2 and ZL55-SO-P10 cells (selected with 2 or 10 μg/mL of puromycin, respectively) compared with the non-selected ZL55-SO cells. *OCT4* levels are increased 1.9-fold in -P2 and nearly 6-fold in the -P10 cells. A significant increase in the expression of *ABCG2* as well as *CSF1R* is detected. Statistical comparisons were performed using a one-way ANOVA (*$p < 0.05$) from three independent experiments; error bars represent SD. See also Figure S1.

proliferation in non-enriched CSC cells, while high SOX2/OCT4-expressing cells selected by the reporter approach were barely affected by forced NF2 expression. Injection of the EGFP(+) cells resulted in an increased frequency, number, and size of tumors in vivo compared with cells with low SOX2/OCT4 expression. These results are indicative of a CSC-enriched population in MM cell lines of human and mouse origin likely relevant for tumor relapse.

RESULTS

Identification and Initial Characterization of High SOX2/OCT4-Expressing Human CSC-Enriched MM Cells

To identify putative CSCs in MM, we relied on a tool initially developed for stem cell biology (Hotta et al., 2009). In this lentivirus-based approach, MM cells of human and mouse origin were infected with a construct that contains SOX2- and OCT4-binding sites in the promoter region, followed by an expression cassette coding for EGFP and an IRES connecting to a puromycin-resistance cassette (Figure 1A). Thus, cells expressing high levels of SOX2/OCT4 can be identified by EGFP expression and, moreover, selected/isolated by their puromycin resistance and/or by FACS. The overall lentiviral transduction efficiency in MM cell lines was assessed with a constitutive NLS-mCherry construct (Figures S1B and S1C). FACS analyses revealed approximately 85% of cells to show red fluorescence; an overlay of bright field and fluorescence images from transduced ZL55 and RN5 MM cells and visual inspection indicated that the transduction efficiency was likely even higher, i.e., in the order of >90% (Figure S1B). In the population of infected ZL55 cells named ZL55-SO cells, we observed approximately 5% of EGFP-expressing (EGFP(+)) cells (Figure 1B). A similar percentage of high SOX2- and OCT4-expressing EGFP(+) cells (ZL55 ≈ 4%; Figure S1A3) was obtained with the SORE6 reporter construct previously

Please cite this article in press as: Blum et al., Stem Cell Factor-Based Identification and Functional Properties of In Vitro-Selected Subpopulations of Malignant Mesothelioma Cells, Stem Cell Reports (2017), http://dx.doi.org/10.1016/j.stemcr.2017.02.005

used in breast cancer cells (Tang et al., 2015). This percentage lies within a similar range to that observed for the ZL55 side population (2% SP cells, Frei et al., 2011) or ALDEFLUOR-positive(+) MM87 cells (3.8%; Shapiro et al., 2014). Quantitative analyses by FACS showed 4.86% of ZL55-SO cells to express sufficiently high levels of SOX2 and OCT4 to drive EGFP expression (Figure 1C). ZL55-SO cells subjected to puromycin (2 μg/mL) selection for 7 days revealed the surviving cell population to show variable EGFP expression and were named ZL55-SO-P2. In order to exclude likely EGFP-negative or low EGFP-expressing cells in the quantitative FACS analyses, based on the stringent FACS settings, 78.6% of ZL55-SO-P2 cells fulfilled the criteria to be unmistakably identified as EGFP(+) cells (Figure 1D); yet, by eye, essentially all cells appeared to emit green fluorescence (Figure 1E). In addition, we generated ZL55-SO-P10 cells, where the puromycin concentration was augmented to 10 μg/mL aimed at selecting cells with the highest levels of SOX2 and OCT4. Expression levels (mRNA) of *SOX2*, *OCT4*, as well as previously proposed MM CSC markers including *ABCG2* and *CSF1R*, all implicated in mesothelioma chemoresistance, were considerably increased (on average 3- to 5-fold) in puromycin-selected ZL55-SO cells (Figure 1F). The largest increase from -P2 to -P10 cells was observed for *OCT4* (Figure 1F). Experiments were carried out with FACS-sorted cells, which were separated based only on their EGFP fluorescence. Details for the sorting are provided in Figure S2A. The identical approach was also used to obtain sorted RN5 cells (Figure S2B). We screened the sorted cells for *ALDH1A1*, *KLF4*, and *c-MYC*, which were all increased in ZL55-SO^{high} cells (Figures S1D and S1E). In the sorted murine RN5-SO^{high} cells, besides *Sox2* and *Oct4*, the stem cell marker *Nanog* was also significantly increased (Figure S1F). A hallmark for putative MM and other tumor type-derived CSCs is their increased resistance toward chemotherapeutic drugs including cis-Pt, as also reported previously for ovarian cancer-derived CSCs (Wiechert et al., 2016). ZL55-SO and ZL55-SO-P2 cells were treated with cis-Pt concentrations ranging from 0.625 to 10 μM, and cell survival was assessed 5 days later (Figure 2A, left panel). Half maximal inhibitory concentration (IC_{50}) values were 0.92 μM for ZL55-SO and 2.13 μM for ZL55-SO-P2 cells, indicating that the EGFP(+) cells displayed higher chemoresistance, i.e., higher survival than the non-selected ZL55-SO cells. While ZL55-SO-P2 cells were almost completely resistant to 1.25 μM cis-Pt as shown by nearly identical growth curves of cis-Pt-exposed and untreated cells, the growth/survival of ZL55-SO cells was considerably impaired under these conditions (Figure 2C). Of note, in ZL55-SO cells, the cells surviving the cis-Pt treatment were to a large extent EGFP(+) cells (Figure 2D) present at about 5% in the non-selected ZL55-SO cells (Figures 1B and 1C). Also, the sorted ZL55-SO^{low} and ZL55-SO^{high} cells were exposed to cis-Pt and IC_{50} values were determined (Figures 2A and 2B). The increase in survival of ZL55-SO^{high} cells compared with ZL55-SO^{low} cells in the presence of cis-Pt was qualitatively similar to that in the puromycin-selected ZL55-SO-P2 versus ZL55-SO cells (Figure 2A). With respect to the increased resistance, the ratio of IC_{50} values for the EGFP(+)-sorted cells (2.7-fold) was slightly higher than for the -SO-P2 versus -SO cells (1.9-fold); the smaller difference in the puromycin-selected cells likely being due to the presence of approximately 5% of EGFP(+) cells in the parental (unsorted) -SO cell population. Sorted cells were also exposed to 5-fluorouracyl (5-FU) and to the FAK inhibitor VS-6063, also known as defactinib. IC_{50} values are summarized in Figure 2B. Of note, no differences were detected in ZL55-SO^{low} and ZL55-SO^{high} cells with respect to their 5-FU sensitivity. In line with previous observations that FAK signaling is increased and functionally relevant in putative CSCs (Shapiro et al., 2014), ZL55-SO^{high} cells were more susceptible toward the FAK inhibitor than the ZL55-SO^{low} cells (Figures 2A and 2B).

SOX2/OCT4-Expressing CSC-Enriched MM Cells Show Stem Cell Properties In Vitro

An essential property of stem cells is asymmetric cell division, i.e., the ability to generate two daughter cells with non-identical properties. We hypothesized that in ZL55-SO-P2 EGFP(+) cells not continuously subjected to puromycin selection or in FACS-sorted ZL55-SO^{high} cells, a fraction of cells would eventually lose EGFP expression, possibly resulting from asymmetric cell division and/or a dynamic switch in CSC differentiation state (Movie S1). While 1 day after puromycin removal essentially all cells were EGFP(+), at later time points (days 6, 71, and 80), first individual EGFP(−) cells and at later stages entire cell clusters of EGFP(−) cells were observed (Figure 3A and Movie S2). Asymmetric cell divisions were documented by time-lapse videos, where mitosis of an EGFP(+) cell resulted in a green and a non-green daughter cell (Movie S1). A decrease of EGFP(+) cells by 13% was observed at day 80 (10 passages) (Figure 3B and Movie S2), and green cells decreased even more after long-term culturing in vitro (data not shown). Their advancement in differentiation from EGFP(+) to EGFP(−) cells was confirmed by their subsequent increased NF2 susceptibility (Movie S4). Of note, within the population of EGFP(+) cells, a second population of cells appeared with a weaker green fluorescence intensity, close to the gating boundaries separating EGFP(+) and EGFP(−) cells (Figure 3B). We conclude that EGFP expression is not based on an all-or-none mechanism, but it exists rather as a continuum of cells with different SOX2/OCT4-based reporters as shown by the heterogeneous EGFP levels possibly resulting from a switch in CSC differentiation state.

Please cite this article in press as: Blum et al., Stem Cell Factor-Based Identification and Functional Properties of In Vitro-Selected Subpopulations of Malignant Mesothelioma Cells, Stem Cell Reports (2017), http://dx.doi.org/10.1016/j.stemcr.2017.02.005

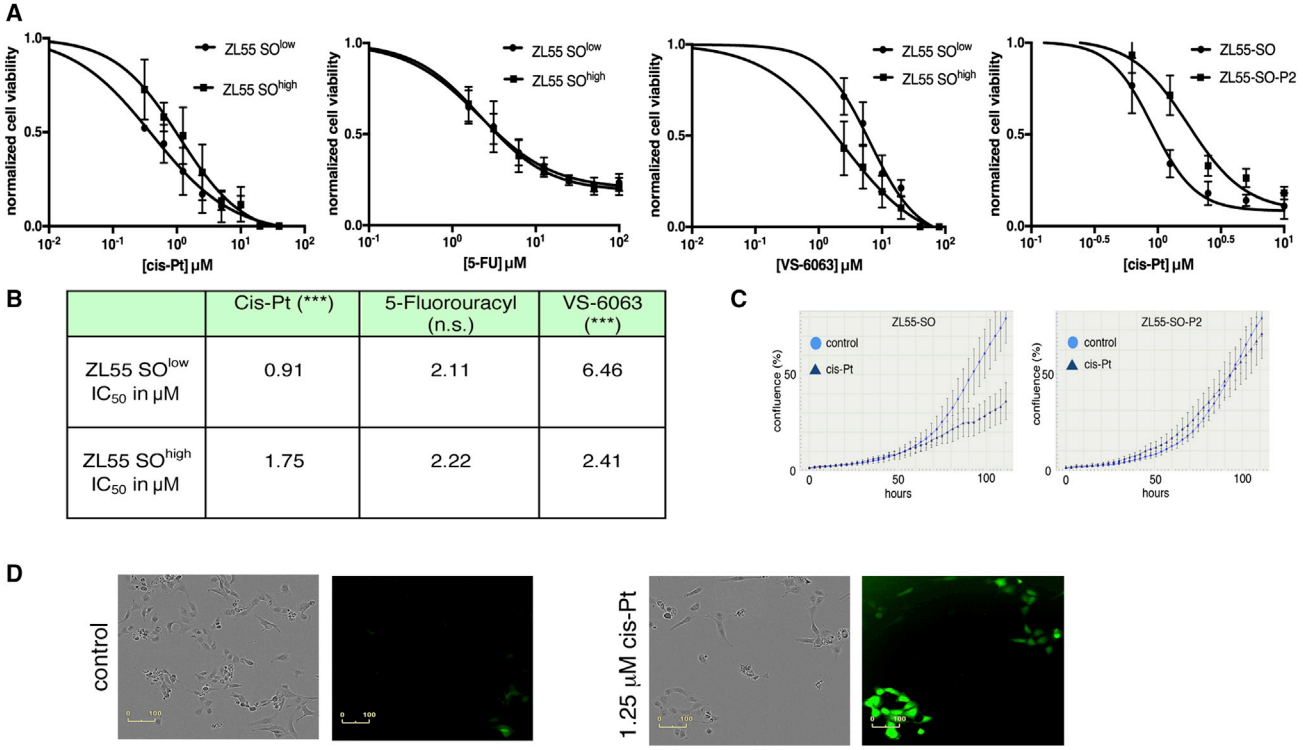

	Cis-Pt (***)	5-Fluorouracyl (n.s.)	VS-6063 (***)
ZL55 SO^{low} IC_{50} in µM	0.91	2.11	6.46
ZL55 SO^{high} IC_{50} in µM	1.75	2.22	2.41

Figure 2. Higher Resistance of ZL55-SO^{high} EGFP(+) Cells Toward cis-Pt and 5-FU and a Lower One Toward VS-6063

(A and B) Increased viability of ZL55-SO-P2 versus ZL55-SO cells exposed to cis-Pt (left panel) (A). From the curves derived from sorted ZL55-SO^{low} and ZL55-SO^{high} cells (right three panels), IC_{50} values for cis-Pt, 5-FU, and VS-6063 were calculated from three independent experiments and are shown in (B). ***$p < 0.001$; one-way ANOVA; n.s., not significant. ZL55-SO^{high} cells display higher susceptibility to VS-6063.

(C) Real-time growth curves show the strong effect of cis-Pt (1.25 µM) on ZL55-SO cell proliferation/survival, while ZL55-SO-P2 cells are almost completely resistant. One representative experiment from three independent experiments.

(D) Bright field and fluorescence images showing the effect of cis-Pt on ZL55-SO cells; the fraction of EGFP(+) cells is increased after cis-Pt exposure (right panels).

SOX2/OCT4-Expressing CSC-Enriched MM Cells Are Present in Cell Lines Derived from All Human MM Histotypes and Also in Murine RN5 MM Cells

Patients with sarcomatoid and biphasic MM have a poorer prognosis than patients diagnosed with an epithelioid MM (Billé et al., 2016). Thus, we set out to investigate whether high SOX2/OCT4-expressing cells were present in cell lines derived from all different MM histotypes and to determine the proportion of EGFP(+) cells. EGFP(+) cell populations were detected in ZL55 (epithelioid), MSTO-211H, SPC111 (biphasic), and murine RN5 (sarcomatoid) cells; their fractions ranged from 4.8% to 7.8% (Table 1). Thus, in all three histotype-derived MM cell lines, EGFP(+), CSC-enriched cell populations were identified. Murine EGFP(+) RN5 cells were used in a syngeneic orthotopic in vivo mouse model aimed at demonstrating that the decrease of EGFP(+) cells observed in culture is not an artifact of in vitro cell culture conditions and/or specific for a certain MM cell line. Sorted RN5-SO^{high} cells were used in an in vivo allograft C57Bl/6J mouse model. Intraperitoneal (i.p.) injection of these cells resulted in tumor nodules after 8 weeks; staining of fixed tumors with a pan-cytokeratin (CK) antibody allowed identification of the tumor cells, further confirmed by double staining for EGFP (Figure 3C). The tumor contained patches of cells with strong EGFP expression, but also regions with weak or absent expression, although these cells were clearly CK positive, i.e., tumor cells. This indicates that a fraction of EGFP(+) tumor cells had lost SOX2/OCT4-driven reporter expression over time in vivo. Furthermore, RN5-SO^{high}-sorted cells were transduced with NLS-mCherry and injected (i.p.) into mice. Tumors were collected after 8 weeks and isolated tumor cells were cultured in vitro for analysis. Among the NLS-mCherry-labeled RN5 MM cells, a fraction of EGFP(−) cells was detected (marked by arrows; Figure 3D). In addition, these NLS-mCherry-transduced RN5-SO^{high} cells were cultured in vitro for an additional 57 days. Cells were analyzed weekly by FACS; the fraction of EGFP(−) cells increased

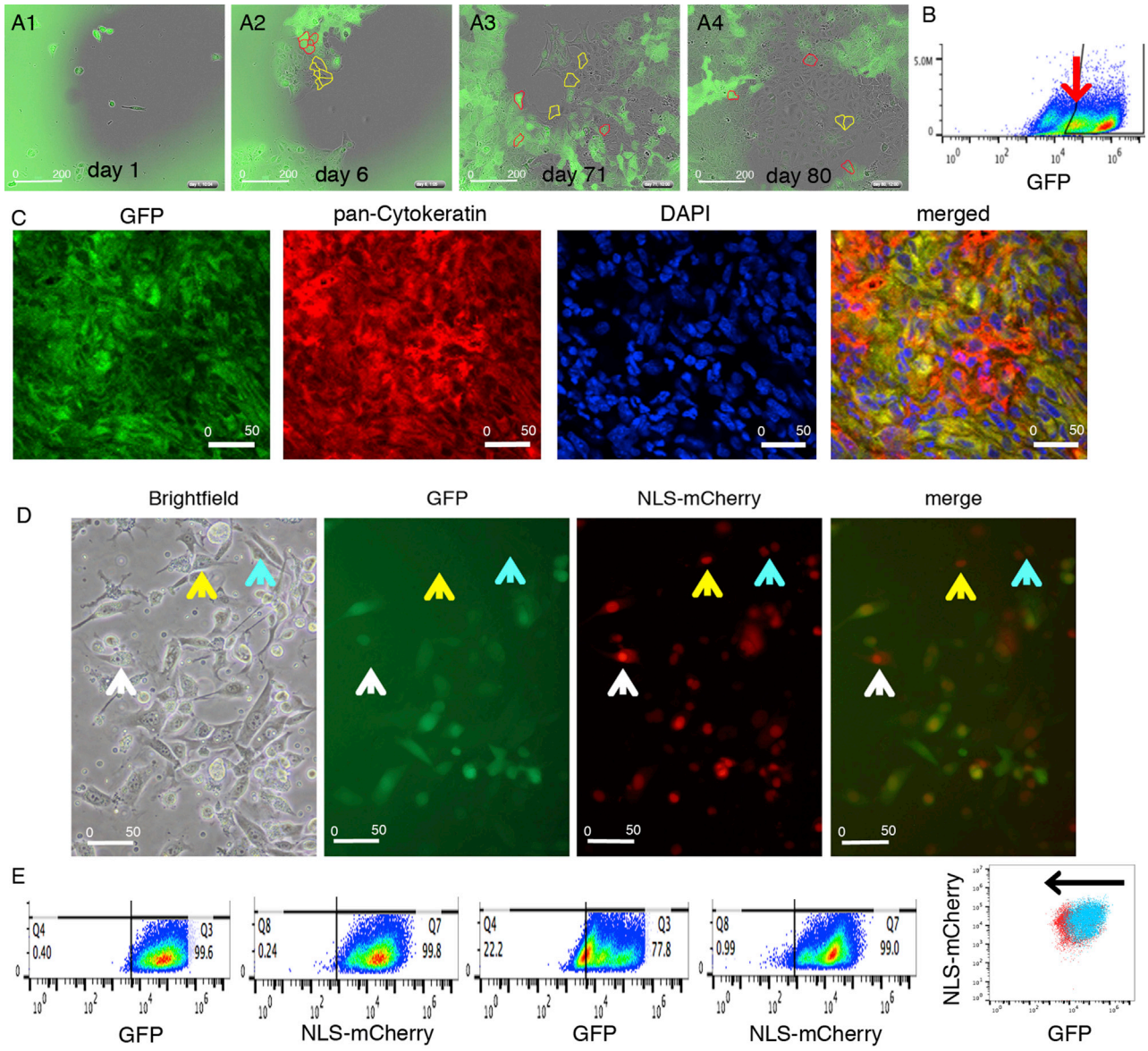

Figure 3. Time-Dependent Decrease in EGFP Expression in Initially 100% EGFP(+) Cells Indicates Gradual Loss of Stemness Observed In Vitro and In Vivo

(A) Example of EGFP(+) and EGFP(−) ZL55-S0 cells in a cell culture dish initially plated with FACS-sorted ZL55-S0^{high} cells. At 80 days in vitro many non-green EGFP(−) cells are observed, often arranged in clusters (marked by yellow dotted lines) and EGFP(+) (examples marked by red dotted lines).

(B) Decrease of the fraction of EGFP(+) cells starting from sorted ZL55-S0^{high} cells (initially 78.6% EGFP(+) cells) to 68.7% after culturing without puromycin selection for 35 days (ten passages). Note the appearance of a distinct population of cells with lower EGFP fluorescence (arrow).

(C) Tumor tissue derived from a mouse injected with RN5-S0^{high} cells for 8 weeks in vivo. In the tumor mass identified by pan-cytokeratin (CK) immunohistochemistry (red fluorescence), clusters of cells with weak-to-none EGFP staining (green fluorescent image; left) are seen. Staining with DAPI (blue) allows better identification of individual cells. In the merged image, the presence of clusters of yellow cells (co-localization of CK and EGFP), but also of cells without EGFP (CK only) demonstrates loss of EGFP expression over time in vivo.

(D) RN5-S0^{high} cells additionally expressing NLS-mCherry (red fluorescent nuclei) formed tumors in vivo as demonstrated after 8 weeks. Tumor-derived cells were cultivated in vitro and revealed that a fraction of NLS-mCherry(+) cells had lost EGFP expression (cells marked by arrows). In the merged image these cells appear as red only.

(legend continued on next page)

Please cite this article in press as: Blum et al., Stem Cell Factor-Based Identification and Functional Properties of In Vitro-Selected Subpopulations of Malignant Mesothelioma Cells, Stem Cell Reports (2017), http://dx.doi.org/10.1016/j.stemcr.2017.02.005

Table 1. Percentage of EGFP(+) Cell Populations in Human and Mouse MM Cell Lines

Cell Line	Origin/Characterization	% GFP(+) Cells
ZL55	human/epithelioid	4.8
SPC111	human/biphasic	6.2
MSTO-211H	human/biphasic	6.1
RN5	murine/sarcomatoid	7.8

from 0.4% to 22.2% after 57 days, while the fraction of NLS-mCherry(−) cells only decreased by 0.8% in the same time period (Figure 3E). An overlay of the green and red cell populations present in cell cultures after 57 days in vitro revealed a left shift of the green cells toward lower fluorescence (increase in EGFP(−) cells), while at the same time the cluster of red cells did not move (Figure 3E). This indicates a selective decrease of EGFP(+) cells over time, i.e., SOX2/OCT4 levels had dropped below the threshold to maintain EGFP expression.

Tumor Growth of ZL55-SO^{high} Cells In Vivo Strongly Indicates CSC Properties

The growth of FACS-sorted ZL55-SO^{low} and ZL55-SO^{high} cells was investigated in vivo in an orthotopic xenograft mouse model. Non-obese diabetic (NOD)/severe combined immunodeficiency (SCID) gamma mice were injected i.p. with 100,000 of either sorted ZL55-SO^{low} or ZL55-SO^{high} cells and the formation of tumor nodules was analyzed 5 weeks after injection. All mice exposed to either cell subpopulation showed macroscopic tumor formations on both the parietal and visceral part of the tunica serosa (Figure 4A). We measured semi-quantitatively the relative surface area covered by tumor tissue; a clearly larger surface area covered by visually discernible tumor nodules after injection of ZL55-SO^{high} cells was observed (Figure 4B). In some cases nearly the entire parietal tunica serosa of mice injected with ZL55-SO^{high} cells was covered with tumor nodules, but to a lesser extent also the visceral tunica serosa of different organs was covered (Figure 4A). The semi-quantitative analyses showed that the tumor-initiating capacity of ZL55-SO^{high} EGFP(+) cells was clearly higher than that of ZL55-SO^{low} EGFP(−) cells. Histological analyses of selected ZL55-SO^{high} tumor nodules showed irregularly formed boundaries between liver tissue and tumor mass, indicative of a highly invasive tumor (Figure 4C).

Characteristics of RN5-SO^{high} Tumor Cell Growth In Vivo Are Different from the One after Injection with RN5-SO^{low} Cells

A limited dilution assay was carried out, where different amounts of FACS-sorted murine MM cells (RN5-SO^{high} and RN5-SO^{low}; 5,000, 50,000, and 500,000 cells per mouse) were injected i.p. in syngeneic C57Bl/6J mice. At three time points 13, 11, and 8 weeks post injection, mice with the largest initial load analyzed after the shortest period were killed and the tumor load/tumor size was investigated semi-quantitatively, first at the macroscopic level and then in more detail on histological sections (Figure 5). Injection of EGFP(−) RN5-SO^{low} cells resulted in the formation of macroscopically discernable tumors in 1 of 12 mice (8.3%); the tumor localization was intramuscular (Figure 5C). More tumors (in 6 of 12 mice; 50%) were detected after injection of RN5-SO^{high} cells; an example of an externally visible tumor of RN5-SO^{high} cells is shown in Figure 5B. Histological analyses revealed that RN5-SO^{high}-derived tumors often localized within the subcutaneous connective tissue, in intramuscular regions of the abdominal wall, but also on the kidney capsule (Figures 5D–5G). Different tissue samples containing small tumor masses from mice injected with either RN5-SO^{high} and RN5-SO^{low} cells were histologically examined. In the RN5-SO^{low} group, tumors were identified in 4 of 12 (33%) mice and clearly more (9 of 12 mice; 75%) in mice injected with RN5-SO^{high} cells (Figure 5A). The tumor incidence in RN5-SO^{high}-injected mice was higher at all three doses of tumor cells tested (Figure 5A). The calculated tumor-initiating frequency using the ELDA software (Hu and Smyth, 2009) for RN5-SO^{high} cells was clearly higher than for RN5-SO^{low} cells (ratio RN5-SO^{high}/RN5-SO^{low}, 17.4; $p = 0.0063$). Thus, also in vivo, EGFP(+) RN5-SO^{high} cells fulfill the criteria of CSC-enriched cells shown by their increased tumor-initiating frequency.

Increased In Vitro Self-Renewal Properties of RN5-SO^{high} and ZL55-SO^{high} Cells Compared with the Corresponding -SO^{low} Subpopulations

Other important CSC characteristics include an augmented capacity for self-renewal and also for anchorage-independent growth in vitro (Morata-Tarifa et al., 2016). Self-renewal was assessed in ZL55 and RN5 cells by a limiting dilution assay as described previously (Tang et al., 2015; Thiagarajan et al., 2015) using sorted -SO^{low} and -SO^{high} cells of both cell types. In both cell lines, the self-renewal capacity of EGFP(+) cells was clearly increased (Figures S3A

(E) Cells shown in (D) were maintained in culture in vitro for an additional 57 days and analyzed by FACS for green (EGFP) and red (NLS-mCherry) fluorescence. While the fraction of NLS-mCherry(+) cells only marginally decreased from 99.8% to 99.0%, the fraction of EGFP(+) cells decreased from 99.6% to 77.8%. Note the left shift of the population of EGFP(+) cells: blue cloud at t1; red cloud at t57. See also Figure S2.

Please cite this article in press as: Blum et al., Stem Cell Factor-Based Identification and Functional Properties of In Vitro-Selected Subpopulations of Malignant Mesothelioma Cells, Stem Cell Reports (2017), http://dx.doi.org/10.1016/j.stemcr.2017.02.005

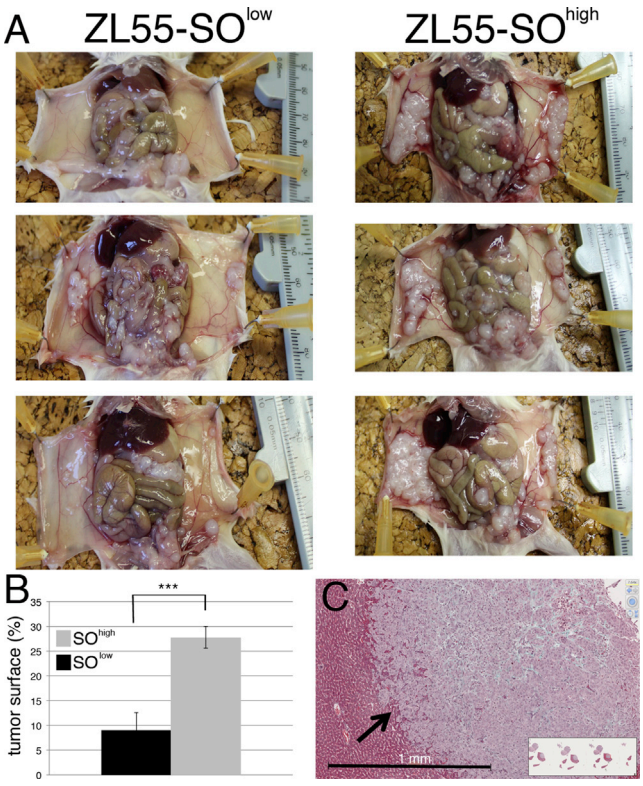

Figure 4. Increased Tumor Growth of Human ZL55-SO^{high} EGFP(+) Cells in NOD/SCID Gamma Mice

(A) ZL55-SO^{low} and ZL55-SO^{high} cells (100,000/mouse) were injected i.p. into NOD/SCID gamma mice. Mice injected with ZL55-SO^{high} cells show an increased number/density of tumor nodules, especially visible on the visceral pleura (right images).

(B) The percentage of tumor nodules covering the surface of the visible parietal and visceral peritoneum is 9.1% for ZL55-SO^{low} cells and 27.8% for ZL55-SO^{high} cells (***$p < 0.001$; one-way ANOVA). Average of four to five animals per group; error bars represent SD.

(C) Tumor masses were histologically analyzed; a tumor nodule on the liver surface shows highly invasive edges (arrow). See also Figure S3.

and S3B). Examples of EGFP(−) and EGFP(+) RN5 tumor spheres initiated from 10 cells/well and maintained in culture for 10 days are shown in Figures S3C and S3D, respectively; the larger size of EGFP(+) tumor spheres was evident. In addition, the anchorage-independent growth in soft agar was investigated in the same cell lines. The average colony size of EGFP(+) RN5-SO^{high} cells after 2 weeks (Figure S3E) was considerably larger than the size of the corresponding EGFP(−) RN5-SO^{low} colonies (Figure S3F). Assuming a spherical shape of the colonies, based on the areas of the colonies depicted in Figures S3E and S3F, the radius of a sphere was calculated. The average radius was significantly larger in RN5-SO^{high} cells than in the RN5-SO^{low} cells (Figure S3H). The differences in radii were smaller between EGFP(−) and EGFP(+) ZL55 cell colonies; however, radii of ZL55-SO^{high} cell colonies were still significantly larger than the ones from EGFP(−) cells (Figure S3G).

Decreased Susceptibility of EGFP(+) ZL55 Cells to Asbestos-Induced Acute Cytotoxicity, but Unaltered Cell Mobility In Vitro

CSCs are known to show higher resistance to exposure to cytotoxic agents (Vidal et al., 2013), possibly linked to their lower proliferation rates, while increased spreading of tumor cells to sites distant from the primary tumor are associated with augmented invasiveness and increased metastatic potential (Anjomshoaa et al., 2009). ZL55-SO-P2 EGFP(+) cells were significantly more resistant toward crocidolite-induced acute cytotoxicity (5 μg/cm^2 of crocidolite for 96 hr) than EGFP(−) cells (Figure 6A). At 96 hr the MTT signal of ZL55-SO-P2 crocidolite-treated cells was only slightly lower than in control ZL55-SO-P2 cells, indicating an almost complete protection of EGFP(+) cells. Real-time growth curves of control ZL55-SO and ZL55-SO-P2 cells did not reveal large differences in the proliferation rates of the two cell populations (Figures 6C and 6D). The MTT signal at 120 hr post-plating for EGFP(−) ZL55-SO^{low} cells was slightly larger than for EGFP(+) ZL55-SO^{high} cells, in line with slower growth of CSCs (data not shown). Yet in a 2D scratch assay, the wound closure time was indistinguishable (data not shown). A more detailed analysis of the mobility of individual cells preferentially toward the cell-devoid area showed a faster cell movement of both cell groups directly following the scratch and lasting for about 2 hr, followed by a constant displacement of approximately 2 μm/5 min for the next 16 hr (Figure S4C). Mobility of ZL55-SO cells grown at low confluence, i.e., allowing for non-directed movement was also not different between EGFP(+) and EGFP(−) cells (Figure S4C). In addition, we used MSTO-211H cells, an MM cell line prone to form spheroids when grown in the absence of serum, to analyze the spheroid formation capacity (Pasdar et al., 2015). MSTO-211H-SO-P2 cells consisting of mostly EGFP(+) cells showed qualitatively a larger number of spheroids (data not shown) that were also bigger than the ones from unsorted MSTO-211H-SO cells (Figures S4A and S4B). Of note, spheroids produced from unsorted MSTO-211H-SO cells containing initially ~7% of EGFP(+) cells were mostly made up of the EGFP(+) cell subpopulation, suggesting that mostly EGFP(+) cells show the propensity of forming spheroids (Figure S4A).

Similar Sensitivity of EGFP(+) and EGFP(−) MM Cells to Calretinin Downregulation, but Pronounced Differences with Respect to Ectopic Expression of the Functional Tumor Suppressor NF2 and to the FAK Inhibitor VS-6063

Although the precise role of the positive MM marker calretinin (*CALB2*) is currently unknown, its downregulation

Please cite this article in press as: Blum et al., Stem Cell Factor-Based Identification and Functional Properties of In Vitro-Selected Subpopulations of Malignant Mesothelioma Cells, Stem Cell Reports (2017), http://dx.doi.org/10.1016/j.stemcr.2017.02.005

A

Cell # (weeks in vivo)	RN5-SO^{low}	RN5-SO^{high}
500'000 (8)	2/4	4/4
50'000 (11)	1/4	3/4
5'000 (13)	1/4	2/4
TIF	1/397'453	1/22'894

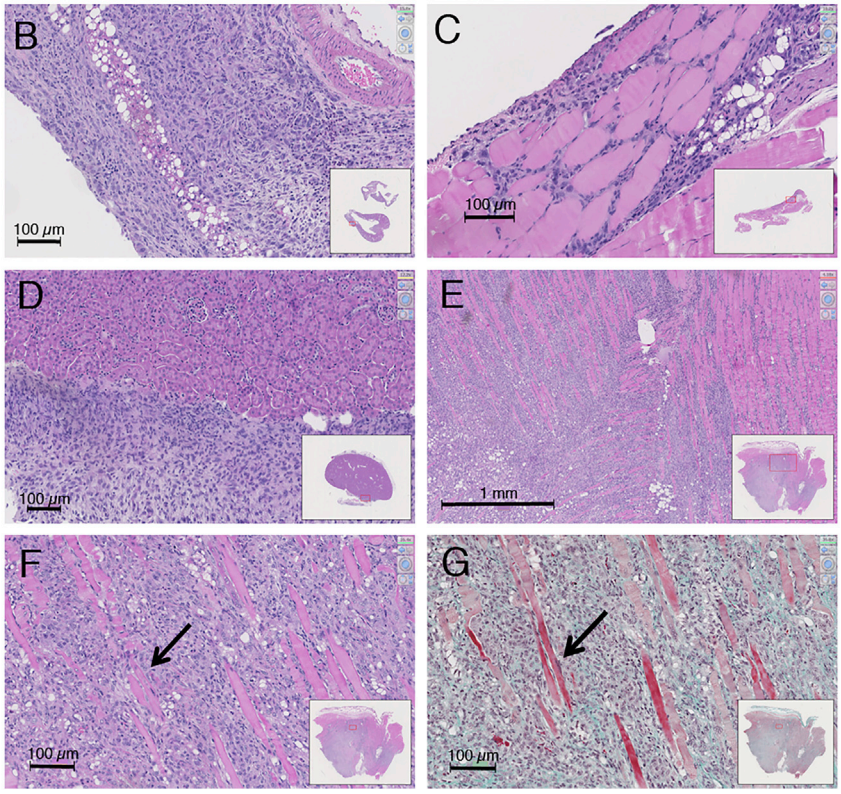

Figure 5. Increased Tumor-Initiating Frequency and Morphological Aspects of RN5-SO^{high} EGFP(+) Cell-Derived Tumors in Syngeneic C57Bl/6J Mice

RN5-SO^{low} and RN5-SO^{high} cells were injected i.p. in C57Bl/6J mice at three doses (500,000, 50,000, and 5,000 cells) and killed after 8, 11, and 13 weeks, respectively.

(A) Fraction of mice with tumors found by microscopic analyses. At all injected doses of RN5 cells and time points, tumor incidence is higher with RN5-SO^{high} cells. The tumor-initiating frequency (TIF) was calculated for both groups.

(B–F) H&E-stained sections. (B) Tumor of RN5-SO^{high} cells (500,000 cells at 8 weeks); tumor cells are located subcutaneously in the parietal wall. (C) Intramuscular tumor in the abdominal wall of the same mouse. (D) In the same group (500,000 cells at 8 weeks), tumor cell growth on the liver surface. (E) and (F) Intramuscular tumors in a mouse (50,000 RN5-SO^{high} cells at 8 weeks).

(G) A parallel section of the one presented in (F) shows a Goldner staining to better emphasize the muscle tissue (red) and the connective tissue (green) in the tumor mass. Arrows in (F) and (G) indicate muscle fibers. See also Figure S3.

in ZL55 cells by a lentivirus-mediated short hairpin RNA (shRNA) approach leads to massive apoptosis and necrosis, most strongly in epithelioid MM (Blum and Schwaller, 2013). Of note, calretinin protein levels were similar in ZL55-SO and ZL55-SO-P2 cells (Figure 6G) and, more importantly, downregulation with shCALB2 no. 5, shCALB2 no. 7 (Blum and Schwaller, 2013), and very efficiently with shCALB2 no. 84 (targeting the CALB2 3′ UTR) affected the survival of ZL55-SO and ZL55-SO-P2 cells to a similar extent (Figure 6B). Thus, unlike the situation with the FAK inhibitor VS-4718 that preferentially affects ALDEFLUOR(+), CSC-enriched MM cells (Shapiro et al., 2014), *CALB2* downregulation equally affected proliferation and viability of ZL55 EGFP(+) and EGFP(−) cells. These results underscore calretinin as an interesting target for the elimination of calretinin-positive MM cells irrespective of their stemness.

Genes that are downregulated or lost in MM and are thought to act as a driver for MM formation include *NF2* (neurofibromatosis 2, merlin), *CDKN2A*, and *BAP1* (Xu et al., 2014). Loss of functional NF2 resulting from mutations is observed in 40%–50% of human MPM (Bianchi et al., 1995) and, moreover, low NF2-expressing MPM cells show a higher sensitivity toward FAK inhibition-induced growth arrest, while NF2 overexpression results in an increased resistance to the FAK inhibitor VS-4718 that preferentially affects ALDEFLUOR(+) CSC-enriched cells (Shapiro et al., 2014). Thus, we investigated how overexpression of human wild-type NF2 affected proliferation and/or survival of EGFP(+) and EGFP(−) MM cells. The proliferation of control ZL55-SO and ZL55-SO-P2 was rather similar, a plateau was reached between 70 and 80 hr after plating (Figures 6C and 6D). Overexpression of NF2 (Figures 6C–6F) selectively affected EGFP(−) ZL55-SO cells, as shown by an almost complete cell growth arrest and cell death (Figures 6C–6F). NF2-overexpressing EGFP(+) ZL55 cells showed the typical epithelioid morphology, while neighboring EGFP(−) cells were characterized by rounding up and cell protrusions typical for dying (apoptotic/necrotic) cells (Figures 6E and 6F; Movies S3 and S4). NF2 upregulation only marginally affected the proliferation of EGFP(+) ZL55-SO-P2 cells (Figure 6D), and the cell

Please cite this article in press as: Blum et al., Stem Cell Factor-Based Identification and Functional Properties of In Vitro-Selected Subpopulations of Malignant Mesothelioma Cells, Stem Cell Reports (2017), http://dx.doi.org/10.1016/j.stemcr.2017.02.005

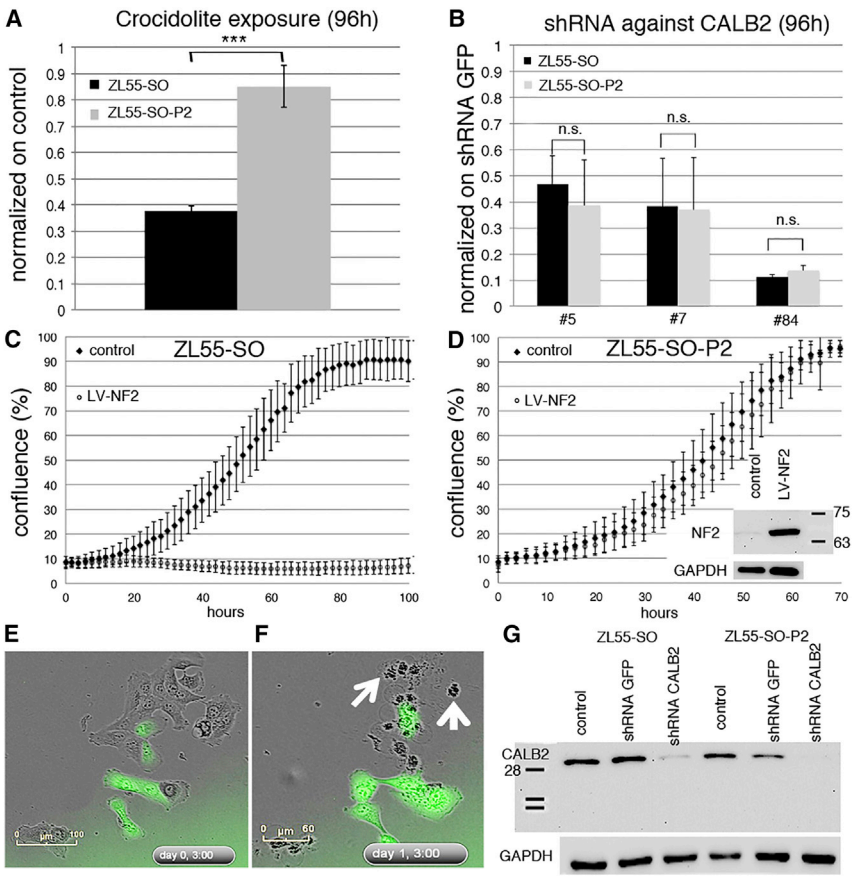

Figure 6. Decreased Susceptibility of EGFP(+) ZL55 Cells to Asbestos Toxicity and NF2 Expression; Equal Sensitivity of EGFP(+) and EGFP(−) ZL55 Cells to Calretinin Downregulation

(A) Increased resistance of ZL55-SO-P2 cells exposed to 5 μg/cm^2 of crocidolite for 96 hr determined by an MTT assay compared with ZL55-SO cells (n = 3 independent experiments, one-way ANOVA; ***p < 0.0005).

(B–D) Downregulation of calretinin in ZL55-SO and ZL55-SO-P2 cells equally decreases the viability in both cell populations for three different shRNA targeting *CALB2* (B) (n = 3 independent experiments; one-way ANOVA; n.s., not significant). Overexpression of merlin (NF2) in ZL55-SO (C) and ZL55-SO-P2 cells (D) shows strong proliferation-inhibiting effects on the non-sorted ZL55-SO cells, but almost no effect on ZL55-SO-P2 cells. The inset in (D) shows strong upregulation of full-length NF2 (M_r = ~68 kDa) using LV-NF2. All error bars represent SD.

(E) Live-cell imaging of ZL55-SO 3 hr after upregulation of NF2; note the presence of EGFP(+) and EGFP(−) cells in the ZL55-SO cell population. The morphology of green and non-green cells is mostly epithelioid.

(F) Twenty-seven hours post infection, the upregulation of NF2 induced strong apoptosis/necrosis in non-green cells (white arrows) demonstrated by cell shrinkage, blebbing, and cell debris. EGFP(+) cells do not show striking morphological changes.

(G) Western blot analysis showing strong downregulation of CR (M_r = 31 kDa) by shRNA CALB2 no. 5 in ZL55-SO and ZL55-SO-P2 cells. At approximately 35 kDa, the nitrocellulose membrane was cut and the upper part was used for GAPDH detection (lower panel). Control infection with shRNA GFP has no effect on CR expression. For the normalization the signal for GAPDH (M_r ~38 kDa) was used. See also Figure S4.

morphology was unaltered (Figures 6E and 6F). Nearly identical results were obtained with human MSTO-211H, SPC111, and ZL5 cells (Figures S4E–S4J). The slow and delayed increase in the proliferation of ZL55-SO-NF2 cells was the result of the low percentage (5%) of EGFP(+) cells present in the unselected (-SO) cells, since nearly all cells were green at 120 hr (Figure S4F). A similar effect was also seen with murine RN5 cells. The smaller magnitude of the effect might be linked to the fact that human, not mouse NF2, was overexpressed in the mouse cells. Thus, in line with previous reports demonstrating that NF2 upregulation in MM cells leads to growth inhibition and apoptosis (Xiao et al., 2005), NF2 overexpression blocked proliferation only in -SO cells mostly consisting of EGFP(−) cells, while barely affecting EGFP(+) cells. Thus, in contrast to the EGFP(−) cells, the CSC-enriched population derived from all MM histotypes was rather insensitive to NF2 overexpression. On the other hand, the FAK inhibitor VS-6063 more efficiently decreased cell proliferation in ZL55-SO-P2 EGFP(+) cells compared with ZL55-SO cells (Figures 2A and 2B).

DISCUSSION

MM are exceptionally resistant to therapeutic interventions such as chemotherapy, radiotherapy, surgery, and combinations thereof. In many instances therapy resistance is linked to a particular microenvironment (Klemm and Joyce, 2015) created and maintained by the tumor tissue and, moreover, by the heterogeneity of the tumor cells within the tumor mass (Bedard et al., 2013). A small subpopulation of cancer cells with stem cell features termed CSCs, or functionally defined as TICs, is assumed to play a crucial role in the development of cancer and in promoting its sustained growth and the invasive and

Please cite this article in press as: Blum et al., Stem Cell Factor-Based Identification and Functional Properties of In Vitro-Selected Subpopulations of Malignant Mesothelioma Cells, Stem Cell Reports (2017), http://dx.doi.org/10.1016/j.stemcr.2017.02.005

metastatic properties (Raggi et al., 2015). Evidence has accumulated that these CSCs are characterized by higher levels of pluripotency factors including SOX2, OCT4, and NANOG. Based on this, methods have been developed to isolate this cell subpopulation as applied in our study. Other approaches to isolate/enrich CSCs exploit specific properties such as enhanced levels of dye-exclusion transporters (*ABCG2*), increased aldehyde dehydrogenase activity (*ALDH1*), or their increased propensity to generate spheroids (Pasdar et al., 2015). While the latter methods might modify these cells to some extent by the selection method, the SOX2/OCT4 reporter approach minimally perturbs the endogenous intracellular environment (excluding the putative effects exerted by EGFP); it allows the identification and isolation of putative CSCs based on their endogenously elevated levels of SOX2/OCT4. Higher levels of SOX2 in glioblastoma were linked with an increased tumor-initiating ability (Gangemi et al., 2009), in ovarian carcinoma associated with the stem cell state, and, in lung cancer, CSCs were required for growth and metastatic potential (Xiang et al., 2011). Moreover, elevated levels of OCT4 and other stemness markers in MM cells derived from mesospheres were paralleled by an increased tumor-initiating capacity (Pasdar et al., 2015). Reporter approaches based on pluripotency factor binding have been successfully used for the enrichment and identification of CSCs in breast cancer (Tang et al., 2015; Thiagarajan et al., 2015) and ovarian cancer (Wiechert et al., 2016), the latter using a NANOG-based reporter. Strong EGFP expression in the lentivirus-mediated SOX2/OCT4-based reporter approach allowed us to isolate and characterize MM cells in vitro and furthermore to investigate in detail the properties of these cells in vivo. One of the main advantages of the reporter approach is the possibility of continuously monitoring these cells over time. This revealed that a fraction of initially EGFP(+) cells lost their green fluorescence, likely as the result of a decrease in SOX2/OCT4 levels insufficient to drive EGFP expression; time-lapse movies demonstrated this loss to occur often within one cell division. We attribute this to a dynamic shift in the differentiation state from EGFP(+) to EGFP(−) cells, the latter characterized by a more non-CSC phenotype as described in detail for breast cancer CSCs (see Figure 7D in Akrap et al., 2016). In agreement, the newly formed EGFP(−) cells were again equally susceptible to the anti-proliferative/pro-apoptotic action of elevated levels of NF2 as were the parental -SO EGFP(−) cells. This precludes the loss of EGFP being the result of, e.g., reporter silencing. This conclusion is also supported by the finding that the same MM cells constitutively expressing NLS-mCherry did not lose red fluorescence over time.

MM are considered as an example, where tumorigenesis is mostly driven by loss of tumor suppressor functions including genes such as *NF2* coding for merlin, *CDKN2A*, *CDKN2B*, or *BAP1* (Jean and Jaurand, 2015). Accordingly, *NF2* is mutated in approximately 40% of all human MM (Bianchi et al., 1995) and/or completely absent by allelic loss (Cheng et al., 1999). NF2 expression levels are strongly correlated with the sensitivity to inhibitors of FAK phosphorylation (Shapiro et al., 2014). The FAK inhibitor VS-4718 efficiently inhibits proliferation of NF2(−) MM cells, while NF2(+) cells are rather insensitive to the inhibitor.

In our study, we compared the sensitivity of EGFP(+) and EGFP(−) MM cells with the effects of overexpression of NF2. In human NF2-overexpressing MM -SO cells, proliferation was almost completely blocked, while EGFP(+) CSC-enriched MM cell populations were barely affected by increased NF2 levels. This effect was completely independent from the NF2 status of the parental cells. NF2-negative ZL55 cells were equally affected, as were NF2-positive MSTO-211H cells. The apparently weaker effect in MSTO-211H-SO cells seen in the real-time growth curves (Figure S4J) is essentially the result of the insensitivity of the small subpopulation of EGFP(+) MSTO-211H-SO cells to NF2 overexpression. Adenovirus-mediated expression of NF2 was previously shown to inhibit proliferation and to cause a G1 cell-cycle arrest in NF2-deficient tumor cells (Xiao et al., 2005). Detailed analyses of NF2-overexpressing ZL55-SO mostly comprising EGFP(−) cells revealed not only a proliferation-inhibiting effect, but considerable cell death caused by elevated NF2 levels. Inhibition of FAK signaling by VS-6063 preferentially affected EGFP(+) ZL55 cells, indicating that a direct impairment of FAK signaling in CSC-enriched ZL55 cells might be the more promising strategy than the likely indirect effect on FAK signaling inhibition by NF2 upregulation that mostly affected the EGFP(−) ZL55 cells.

Since downregulation of calretinin decreases the viability and proliferation of MM cells in vitro (Blum and Schwaller, 2013), we investigated the effects of decreasing calretinin expression in EGFP(+) and EGFP(−) cells. Interestingly, shRNA CALB2-mediated downregulation equally affected both cell populations with respect to proliferation and cell death. Thus, calretinin remains an interesting target to eradicate both MM CSCs and non-CSCs.

The limited dilution assay remains the gold standard for the identification and characterization of CSC- or TIC-enriched cell populations. Here we have chosen two orthotopic i.p. models presuming that tumor cells encounter an environment that is more relevant with respect to human MM pathology (a lumen covered by the mesothelium) than in the more often used subcutaneous models (Pasdar et al., 2015; Shapiro et al., 2014). In the xenograft model using human ZL55 cells, formation of tumor nodules covering the parietal as well as the visceral mesothelium

Please cite this article in press as: Blum et al., Stem Cell Factor-Based Identification and Functional Properties of In Vitro-Selected Subpopulations of Malignant Mesothelioma Cells, Stem Cell Reports (2017), http://dx.doi.org/10.1016/j.stemcr.2017.02.005

was clearly increased when injecting EGFP(+) cells in comparison with injection-treated with unsorted ZL55, comprising less than 5% of EGFP(+) cells. In the physiologically more relevant allograft model using C57BL/6J mice characterized by their highly competent immune system and the previously established mouse MM cell line RN5 (Blum et al., 2015), the tumor-initiating capacity of EGFP(+) RN5 cells was almost 20-fold higher than that of EGFP(−) RN5 cells. Of note, the initial tumor cell load to induce i.p. tumor nodules with RN5 cells was significantly higher than the number of mouse MM87 cells that were injected subcutaneously (s.c.) in the NOD/SCID mouse model (Shapiro et al., 2014). To summarize, both normal (C57BL/6J) versus compromised (NOD/SCID) immune system cells, and orthotopic versus s.c. injection cells, might contribute to the higher tumor cell (RN5) load required for MM formation in vivo.

In comparison with CSCs from tumors derived from other tissues, the nature of MM CSCs with respect to niche, interactions with the microenvironment, and most importantly the immune system and other properties in vivo are as yet under exploited. We estimate that the EGFP-based approach will allow also to visualize EGFP(+) cell fate in the intact tumor microenvironment in the pleural or peritoneal cavities, e.g., for detailed longitudinal studies in vivo. In most previous studies, e.g., involvement of SOX2 in self-renewal (Arnold et al., 2011) or tumor-initiating capability (Gangemi et al., 2009) and the role of OCT4 in dedifferentiation and stemness of cancer cells (Kumar et al., 2012) has been investigated separately. Finally, we propose that the same approach might be applied for primary (non-transformed) mesothelial cells. Such studies might shed light on the role of normal mesothelial stem cells in the process of transformation to MM. The insights into MM CSC biology provided here are expected to be relevant in the search for innovative approaches to target this critically important MM cell population.

EXPERIMENTAL PROCEDURES

Cell Culture and Selection of SOX2/OCT4-Expressing Cells

MM cell lines were cultured as described above, transduced with lentivirus containing SOX2/OCT4 stemness indicator constructs (for details, see the Supplemental Experimental Procedures) resulting in "MM-SO" cells consisting of EGFP(+) and EGFP(−) subpopulations. Treatment with either 2 or 10 μg/mL of puromycin for 10 days led to an enrichment of EGFP(+) cells. In some experiments, ZL55-SO cells were exposed to 2 or 10 μg/mL of puromycin for 3 weeks, followed by a growth period of 3 weeks (10 passages) without puromycin. Cells were then analyzed by flow cytometry for EGFP expression.

Flow Cytometry Analysis of EGFP(+) Cells

Trypsinized MM cells were analyzed by FACS on a BD Accuri C6 (BD Biosciences); details are described in the Supplemental Experimental Procedures. Sorting of EGFP(+) and EGFP(−) cells was performed on a BD FACSAria (BD Biosciences) cell sorter and selected cells were used for subsequent cell culture experiments in vitro.

Determination of the mRNA Expression of Stemness Gene Levels by qRT-PCR

Total RNA extracted from 80% confluent cell cultures (peqGOLD TriFast) of puromycin-selected or sorted ZL55-SO or RN5-SO cells was used for qRT-PCR following the manufacturer's instructions (QIAGEN). qRT-PCR primer sequences are listed in the Supplemental Experimental Procedures.

Treatment of Cells with cis-Pt, 5-FU, and VS-6063 and Determination of IC_{50} Values

Cells (500/well for cis-Pt and 5-FU experiments and 2,000/well for VS-6063) were seeded in 96-well plates and grown for 24 hr. Drugs were added at different concentrations (for details, see the Supplemental Experimental Procedures) and the MTT assay was performed at 48, 96, or 120 hr post treatment (depending on the drug) to determine IC_{50} values. Additionally, real-time cell-proliferation curves were acquired with the IncuCyte Live-Cell Imaging System (Essen BioScience).

In Vivo Limiting Dilution Assay

Animal experiments were performed with the permission of the local animal care committee (Canton of Fribourg, Switzerland) and according to the present Swiss law and the European Communities Council Directive of 24 November 1986 (86/609/EEC). Murine RN5-SO^{low} and RN5-SO^{high} cells were resuspended in 200 μL PBS and injected i.p. in C57Bl/6J mice (four mice per group, three different concentrations). Cells (5,000, 50,000, and 500,000) were injected and groups killed in parallel after 13, 11, and 8 weeks, respectively. Photographs were taken to show macroscopic tumor appearance. Organ samples were collected (diaphragm, spleen, liver, and peritoneal wall) for histological analysis. Sorted ZL55-SO^{low} and ZL55-SO^{high} cells (100,000/mouse) were injected into NOD/SCID gamma mice (four to five mice per group).

Western Blot Assays for Calretinin, NF2, and Mesothelin

Proteins were extracted from washed cell pellets (from 70% to 90% confluent cultures) using standard RIPA buffer (for details, see the Supplemental Experimental Procedures). From the cleared supernatant, proteins (50 μg) were separated on 10% polyacrylamide SDS gels and transferred onto nitrocellulose membranes. After blocking, membranes were first incubated with antibodies against calretinin, mesothelin, or NF2, followed by the ABC detection system using the horseradish peroxidase substrate (Millipore, Luminata Forte); membranes were imaged on the western blot reader FluorChem E System (Bucher Biotec).

Downregulation of Calretinin in ZL55-SO and ZL55-SO-P2 Using Lentiviral-Mediated CALB2 shRNA and Upregulation of NF2

Cells (500/well in 96-well plates) were grown for 24 hr and transduced with lentivirus shRNA CALB2 nos. 5 and 7 (Blum and Schwaller, 2013) or a novel 3′ UTR-targeted shRNA CALB2: 5′-CCG GTT TAA CGC GAT CTT CAC ATT TCT CGA GAA ATG TGA AGA TCG CGT TAA ATT TTT TG-3′. MTT assays were performed at 120 hr post infection. For NF2 upregulation, cells were transduced with LV-NF2 and growth curves were determined by the IncuCyte system.

SUPPLEMENTAL INFORMATION

Supplemental Information includes Supplemental Experimental Procedures, four figures, and four movies and can be found with this article online at http://dx.doi.org/10.1016/j.stemcr.2017.02.005.

ACKNOWLEDGMENTS

The authors thank V. Salicio, S. Eichenberger, M. Sanchez, M. Steinauer, and F. Meyenhofer for their excellent technical assistance, and T. Henzi, V. Szabolcsi, F. Filice, J. Wörthmüller-Rodriguez, and V. Serre-Beinier, University of Geneva, for feedback on the manuscript. PL-SIN-EOS-S(4+)-EiP was a gift from J. Ellis (Addgene plasmid no. 21314) and the SORE6 constructs were a kind gift of Dr. L.M. Wakefield. The project was supported by the Swiss National Science Foundation SNF grant nos. 130680 and 139226 to B.S., San Salvatore Foundation and SNF Sinergia grant no. 147697 to E.F.-B., M.d.P., and B.S.

Received: July 18, 2016
Revised: February 6, 2017
Accepted: February 7, 2017
Published: March 9, 2017

REFERENCES

Akrap, N., Andersson, D., Bom, E., Gregersson, P., Ståhlberg, A., and Landberg, G. (2016). Identification of distinct breast cancer stem cell populations based on single-cell analyses of functionally enriched stem and progenitor pools. Stem Cell Rep. *6*, 121–136.

Anjomshoaa, A., Nasri, S., Humar, B., McCall, J.L., Chatterjee, A., Yoon, H.-S., McNoe, L., Black, M.A., and Reeve, A.E. (2009). Slow proliferation as a biological feature of colorectal cancer metastasis. Br. J. Cancer *101*, 822–828.

Arnold, K., Sarkar, A., Yram, M.A., Polo, J.M., and Bronson, R. (2011). Sox2+ adult stem and progenitor cells are important for tissue regeneration and survival of mice. Cell Stem Cell *9*, 317–329.

Bedard, P.L., Hansen, A.R., Ratain, M.J., and Siu, L.L. (2013). Tumour heterogeneity in the clinic. Nature *501*, 355–364.

Bianchi, A.B., Mitsunaga, S.I., Cheng, J.Q., Klein, W.M., Jhanwar, S.C., Seizinger, B., Kley, N., Klein-Szanto, A.J., and Testa, J.R. (1995). High frequency of inactivating mutations in the neurofibromatosis type 2 gene (NF2) in primary malignant mesotheliomas. Proc. Natl. Acad. Sci. USA *92*, 10854–10858.

Billé, A., Krug, L.M., Woo, K.M., Rusch, V.W., and Zauderer, M.G. (2016). Contemporary analysis of prognostic factors in patients with unresectable malignant pleural mesothelioma. J. Thorac. Oncol. *11*, 249–255.

Blum, W., and Schwaller, B. (2013). Calretinin is essential for mesothelioma cell growth/survival in vitro: a potential new target for malignant mesothelioma therapy? Int. J. Cancer *133*, 2077–2088.

Blum, W., Pecze, L., Felley-Bosco, E., Worthmüller-Rodriguez, J., Wu, L., Vrugt, B., de Perrot, M., and Schwaller, B. (2015). Establishment of immortalized murine mesothelial cells and a novel mesothelioma cell line. In Vitro Cell Dev. Biol. Anim. *51*, 714–721.

Cheng, J.Q., Lee, W.C., Klein, M.A., Cheng, G.Z., Jhanwar, S.C., and Testa, J.R. (1999). Frequent mutations of NF2 and allelic loss from chromosome band 22q12 in malignant mesothelioma: evidence for a two-hit mechanism of NF2 inactivation. Genes Chromosomes Cancer *24*, 238–242.

Cho, B.C.J., Feld, R., Leighl, N., Opitz, I., Anraku, M., Tsao, M.-S., Hwang, D.M., Hope, A., and de Perrot, M. (2014). A feasibility study evaluating Surgery for Mesothelioma after Radiation Therapy: the "SMART" approach for resectable malignant pleural mesothelioma. J. Thorac. Oncol. *9*, 397–402.

D'Angelo, R.C., and Wicha, M.S. (2010). Stem cells in normal development and cancer. Prog. Mol. Biol. Transl Sci. *95*, 113–158.

Frei, C., Opitz, I., Soltermann, A., Fischer, B., Moura, U., Rehrauer, H., Weder, W., Stahel, R., and Felley-Bosco, E. (2011). Pleural mesothelioma side populations have a precursor phenotype. Carcinogenesis *32*, 1324–1332.

Gangemi, R.M.R., Griffero, F., Marubbi, D., Perera, M., Capra, M.C., Malatesta, P., Ravetti, G.L., Zona, G.L., Daga, A., and Corte, G. (2009). SOX2 silencing in glioblastoma tumor-initiating cells causes stop of proliferation and loss of tumorigenicity. Stem Cells *27*, 40–48.

Hirschmann-Jax, C., Foster, A.E., Wulf, G.G., Nuchtern, J.G., Jax, T.W., Gobel, U., Goodell, M.A., and Brenner, M.K. (2004). A distinct "side population" of cells with high drug efflux capacity in human tumor cells. Proc. Natl. Acad. Sci. USA *101*, 14228–14233.

Hotta, A., Cheung, A.Y.L., Farra, N., Garcha, K., Chang, W.Y., Pasceri, P., Stanford, W.L., and Ellis, J. (2009). EOS lentiviral vector selection system for human induced pluripotent stem cells. Nat. Protoc. *4*, 1828–1844.

Hu, Y., and Smyth, G.K. (2009). ELDA: extreme limiting dilution analysis for comparing depleted and enriched populations in stem cell and other assays. J. Immunol. Methods *347*, 70–78.

Jean, D., and Jaurand, M.-C. (2015). Causes and pathophysiology of malignant pleural mesothelioma. Lung Cancer Manag *4*, 219–229.

Klemm, F., and Joyce, J.A. (2015). Microenvironmental regulation of therapeutic response in cancer. Trends Cell Biol. *25*, 198–213.

Klonisch, T., Wiechec, E., Hombach-Klonisch, S., Ande, S.R., Wesselborg, S., Schulze-Osthoff, K., and Los, M. (2008). Cancer stem cell markers in common cancers – therapeutic implications. Trends Mol. Med. *14*, 450–460.

Kumar, S.M., Liu, S., Lu, H., Zhang, H., Zhang, P.J., Gimotty, P.A., Guerra, M., Guo, W., and Xu, X. (2012). Acquired cancer stem

cell phenotypes through Oct4-mediated dedifferentiation. Oncogene *31*, 4898–4911.

Morata-Tarifa, C., Jimenez, G., Garcia, M.A., Entrena, J.M., Grinan-Lison, C., Aguilera, M., Picon-Ruiz, M., and Marchal, J.A. (2016). Low adherent cancer cell subpopulations are enriched in tumorigenic and metastatic epithelial-to-mesenchymal transition-induced cancer stem-like cells. Scientific Rep. *6*, 18772.

Pasdar, E.A., Smits, M., Stapelberg, M., Bajzikova, M., Stantic, M., Goodwin, J., Yan, B., Stursa, J., Kovarova, J., Sachaphibulkij, K., et al. (2015). Characterisation of mesothelioma-initiating cells and their susceptibility to anti-cancer agents. PLoS One *10*, e0119549.

Raggi, C., Mousa, H.S., Correnti, M., Sica, A., and Invernizzi, P. (2015). Cancer stem cells and tumor-associated macrophages: a roadmap for multitargeting strategies. Oncogene *35*, 671–682.

Shapiro, I.M., Kolev, V.N., Vidal, C.M., Kadariya, Y., Ring, J.E., Wright, Q., Weaver, D.T., Menges, C., Padval, M., McClatchey, A.I., et al. (2014). Merlin deficiency predicts FAK inhibitor sensitivity: a synthetic lethal relationship. Sci. Translational Med. *6*, 237ra68.

Stahel, R.A., Felley-Bosco, E., Opitz, I., and Weder, W. (2009). Malignant pleural mesothelioma. Future Oncol. *5*, 391–402.

Tang, B., Raviv, A., Esposito, D., Flanders, K.C., Daniel, C., Nghiem, B.T., Garfield, S., Lim, L., Mannan, P., Robles, A.I., et al. (2015). A flexible reporter system for direct observation and isolation of cancer stem cells. Stem Cell Rep. *4*, 155–169.

Thiagarajan, P.S., Hitomi, M., Hale, J.S., Alvarado, A.G., Otvos, B., Sinyuk, M., Stoltz, K., Wiechert, A., Mulkearns-Hubert, E., Jarrar, A.M., et al. (2015). Development of a fluorescent reporter system to delineate cancer stem cells in triple-negative breast cancer. Stem Cells *33*, 2114–2125.

Valent, P., Bonnet, D., De Maria, R., Lapidot, T., Copland, M., Melo, J.V., Chomienne, C., Ishikawa, F., Schuringa, J.J., Stassi, G., et al. (2012). Perspectives. Nat. Rev. Cancer *12*, 767–775.

Vidal, S.J., Rodriguez-Bravo, V., Galsky, M., Cordon-Cardo, C., and Domingo-Domenech, J. (2013). Targeting cancer stem cells to suppress acquired chemotherapy resistance. Oncogene *33*, 4451–4463.

Visvader, J.E., and Lindeman, G.J. (2008). Cancer stem cells in solid tumours: accumulating evidence and unresolved questions. Nat. Rev. Cancer *8*, 755–768.

Wiechert, A., Saygin, C., Thiagarajan, P.S., Rao, V.S., Hale, J.S., Gupta, N., Hitomi, M., Nagaraj, A.B., DiFeo, A., Lathia, J.D., and Reizes, O. (2016). Cisplatin induces stemness in ovarian cancer. Oncotarget *7*, 30511–30522.

Xiang, R., Liao, D., Cheng, T., Zhou, H., Shi, Q., Chuang, T.S., Markowitz, D., Reisfeld, R.A., and Luo, Y. (2011). Downregulation of transcription factor SOX2 in cancer stem cells suppresses growth and metastasis of lung cancer. Br. J. Cancer *104*, 1410–1417.

Xiao, G.-H., Gallagher, R., Shetler, J., Skele, K., Altomare, D.A., Pestell, R.G., Jhanwar, S., and Testa, J.R. (2005). The NF2 tumor suppressor gene product, merlin, inhibits cell proliferation and cell cycle progression by repressing cyclin D1 expression. Mol. Cell Biol. *25*, 2384–2394.

Xu, J., Kadariya, Y., Cheung, M., Pei, J., Talarchek, J., Sementino, E., Tan, Y., Menges, C.W., Cai, K.Q., Litwin, S., et al. (2014). Germline mutation of Bap1 accelerates development of asbestos-induced malignant mesothelioma. Cancer Res. *74*, 4388–4397.